FEBS Letters 352 (1994) 251–257

FEBS 14554

NMR solution structure of the recombinant tick anticoagulant protein (rTAP), a factor Xa inhibitor from the tick *Ornithodoros moubata*

W. Antuch[a], P. Güntert[a], M. Billeter[a], T. Hawthorne[b], H. Grossenbacher[b], K. Wüthrich[a,*]

[a]*Institut für Molekularbiologie und Biophysik, Eidgenössische Technische Hochschule-Hönggerberg, CH-8093 Zürich, Switzerland*
[b]*Biotechnology Department, Ciba-Geigy AG, CH-4002 Basel, Switzerland*

Received 15 August 1994

Abstract The solution structure of the recombinant tick anticoagulant protein (rTAP) was determined by ^{1}H nuclear magnetic resonance (NMR) spectroscopy in aqueous solution at pH 3.6 and 36°C. rTAP is a 60-residue protein functioning as a highly specific inhibitor of the coagulation protease factor Xa, which was originally isolated from the tick *Ornithodoros moubata*. Its regular secondary structure consists of a two-stranded antiparallel β-sheet with residues 22–28 and 32–38, and an α-helix with residues 51–60. The relative orientation of these regular secondary structure elements has nearly identical counterparts in the bovine pancreatic trypsin inhibitor (BPTI). In contrast, the loop between the β-sheet and the C-terminal α-helix as well as the N-terminal 20-residue segment preceding the β-sheet adopt different three-dimensional folds in the two proteins. These observations are discussed with regard to the implication of different mechanisms of protease inhibition by rTAP and by Kunitz-type protein proteinase inhibitors.

Key words: Tick anticoagulant protein; Protein structure; Nuclear magnetic resonance; Blood coagulation; Proteinase inhibitor

1. Introduction

A crucial step in blood coagulation is the conversion of prothrombin into its active form, thrombin. Efficient proteolytic cleavage of prothrombin by factor Xa is achieved in a Ca^{2+}-dependent assembly of prothrombin, factor Va and factor Xa on phospholipid membrane surfaces. Thrombin then converts fibrinogen into fibrin, which together with activated platelets forms clots that impede blood loss [1,2]. Regulation of the proteolytic enzymes of the coagulation cascade has long attracted much interest. Hirudin, a thrombin inhibitor from the leech *Hirudo medicinalis* [3], has been extensively studied and its structure has been solved in the free form by nuclear magnetic resonance (NMR) spectroscopy [4–6] and in complexes with thrombin by X-ray crystallography [7,8]. Antistasin [9], ghilanten [10], trypstatin [11] and tick anticoagulant protein (TAP) [12] are inhibitors of factor Xa which have all been purified, but no three-dimensional structures have so far been determined. Here we report the NMR solution structure of recombinant TAP (rTAP) and compare this structure with that of Kunitz-type proteinase inhibitors.

TAP was originally isolated from the soft tick *Ornithodoros moubata*. It is a highly selective inhibitor of factor Xa while exhibiting no inhibitory activity against other common serine proteases such as trypsin, chymotrypsin or thrombin [12]. Analysis of the reaction pathway of its inhibitory interaction with factor Xa [13] and site-directed mutagenesis studies suggest a different mode of action from that of the common Kunitz-type proteinase inhibitors [14]. Knowledge of the three-dimensional structure of rTAP should help to obtain a better understanding of the inhibitory mechanism and to further evaluate possible therapeutic applications, all the more since the three-dimensional structure of a truncated form of factor Xa, which lacks the N-terminal 45 residues, has recently also been solved [15].

*Corresponding author. Fax: (41) (1) 633 11 51.

Abbreviations: rTAP, recombinant tick anticoagulant protein; BPTI, bovine pancreatic trypsin inhibitor; Toxin K, dendrotoxin K from *Dendroaspis polylepis polylepis*; α-DTX, α-dendrotoxin from *Dendroaspis angusticeps*; APPI, proteinase inhibitor domain of the Alzheimer's amyloid β-protein precursor; ShPI, Kunitz-type proteinase inhibitor from *Stichodactyla helianthus*; TFA, trifluoroacetic acid; NMR, nuclear magnetic resonance; 2D, two-dimensional; 2QF-COSY, 2D two-quantum-filtered correlation spectroscopy; 3QF-COSY, 2D three-quantum-filtered correlation spectroscopy; 2Q-spectroscopy, 2D two-quantum spectroscopy; TOCSY, 2D total correlation spectroscopy; NOE, nuclear Overhauser effect; NOESY, 2D NOE spectroscopy; E. COSY, 2D exclusive COSY; $^3J_{HN\alpha}$, vicinal spin-spin coupling constant between the amide proton and the α-proton; $^3J_{\alpha\beta}$, vicinal spin–spin coupling constant between the α-proton and a β-proton; CD, circular dichroism; Θ_{MR}, mean residue molar ellipticity.

2. Materials and methods

2.1. Protein preparation

rTAP was expressed with the metallothionein (CUP1) inducible promoter in yeast on a 10-liter scale and purified from the extracellular medium [16]. Centrifuged medium was concentrated using cross-flow membranes (Herasette 14 cm × 14 cm, 3 kDa cutoff, Heraeus Instruments, Zürich). The concentrate was then batch adsorbed to Lichropep Reverse Phase C-18 silica (7 micron particle diameter) (Merck, Darmstadt). Following filtration, the silica was washed sequentially with water and with 15% aqueous CH_3CN containing 0.1% TFA. Active rTAP was eluted in batch mode with 50% aqueous CH_3CN, 0.1% TFA. The eluate was diluted with buffer A (0.1% aqueous TFA) and loaded onto a preparative reverse phase Lichrosphere 100 RP C-18 column (50 × 250 mm, 7 micron particle diameter) on a Sep Tech Nova Prep HPLC. The column was washed with 28% of buffer B (80% aqueous CH_3 CN containing 0.08% TFA) using a flow rate of 80 ml/min, and rTAP was eluted with a linear gradient to 48% buffer B in 44 min. The CH_3CN was removed by rotary evaporation, and the rTAP-containing fractions were pooled and lyophilized. The lyophilizate gave a slightly brown-colored solution in 8% CH_3COOH, which was loaded onto a Sephacryl S-100 column (880 × 25 mm, Pharmacia, Uppsala) equilibrated with 5% CH_3COOH at a flow rate of 1.4 ml/min in order to remove the colored contaminant.

2.2. NMR spectroscopy

NMR spectra were obtained from 8 mM rTAP samples, either in a mixture of 90% H_2O/10% ^2H_2O, or in 99.99% ^2H_2O after complete exchange of all labile protons. The protein samples were adjusted to pH 3.6 by the addition of minute amounts of NaOH and HCl, or NaO^2H and ^2HCl, respectively. The spectra were recorded on Bruker AMX 500 and AMX 600 spectrometers and the temperature of all experiments used for the structure determination was 36.0 ± 0.5°C. In order to assign the proton resonances, homonuclear 2QF-COSY [17], clean-

SSDI 0014-5793(94)00941-4

TOCSY [18] and NOESY [19] (mixing time τ_m = 100 ms) spectra were recorded in both H_2O and ^2H_2O solution, and 3QF-COSY [20] and 2Q-spectra [21] were recorded in ^2H_2O.

The conformational constraints for the structure determination of rTAP were collected from the following 600 MHz spectra: NOE upper bounds on ^1H–^1H distances were obtained from two NOESY experiments with τ_m = 50 ms and selective suppression of zero-quantum coherences [22]. A data set in H_2O solution was recorded with 1,024 × 4,096 complex points, with $t_{1\,max}$ = 76 ms and $t_{2\,max}$ = 303 ms. A data set in ^2H_2O used 650 × 4,096 complex points, with $t_{1\,max}$ = 53 ms and $t_{2\,max}$ = 331 ms. Vicinal spin–spin coupling constants $^3J_{HN\alpha}$ were determined from the aforementioned NOESY spectrum in H_2O by inverse Fourier transformation of in-phase multiplets [23]. Vicinal spin–spin coupling constants $^3J_{\alpha\beta}$ were obtained from an E.COSY spectrum [24] recorded in ^2H_2O with a digital resolution of 1.6 Hz/point along ω_2. The time-domain data were processed on a Bruker X-32 data station using the UXNMR software. The NOESY spectra were weighted with a cosine window and zero-filled about two-fold to 2,048 complex points in t_1 and 8,192 complex points in t_2 prior to Fourier transformation. Baseline distortions in the NOESY spectra were eliminated using the FLATT procedure [25].

The amide proton exchange in rTAP was followed by recording a series of TOCSY [18] spectra at 36°C immediately after the lyophilized protein was dissolved in ^2H_2O at p^{2}H 3.6. The acquisition time of each individual spectrum was 1.5 h.

2.3. *Collection of conformational constraints and determination of the three-dimensional structure*

We followed the procedure outlined in [26] for the input collection and the structure calculation, using the programs XEASY (C. Bartels, T.X. Xia, P. Güntert, M. Billeter and K. Wüthrich, to be published), INFIT [23], CALIBA [27], HABAS [28], GLOMSA [27], DIANA [27,29] and ASNO [30]. Several rounds of structure calculations with DIANA and NOESY cross peak assignments with ASNO were performed. No hydrogen bond constraints were included in the input for DIANA. Disulfide bonds, as determined by chemical methods [31] were constrained in the same way as described in [32]. The final round of DIANA structure calculations was started with 50 randomized conformers and included two REDAC cycles [29]. The resulting 20 DIANA conformers with the smallest residual target function values were subjected to restrained energy minimization using the AMBER force field [33] as implemented in the program OPAL (P. Luginbühl, P. Güntert, M. Billeter and K. Wüthrich, to be published). These 20 energy-refined conformers were used to represent the solution structure of rTAP.

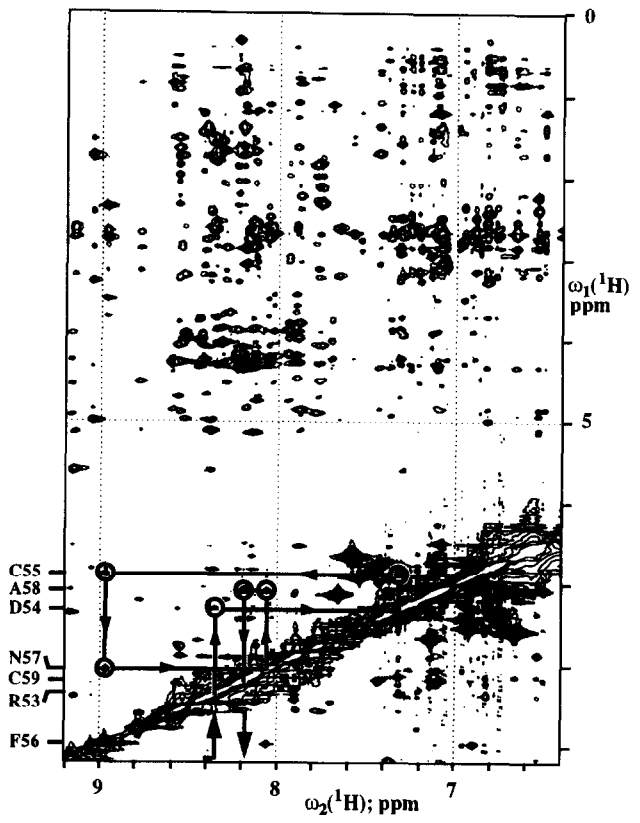

Fig. 2. Contour plot of the spectral region (ω_1 = 0–9.2 ppm, ω_2 = 6.4–9.2 ppm) of a 600 MHz NOESY spectrum of rTAP (protein concentration 8 mM, solvent 90% H_2O/10% ^2H_2O, pH = 3.6, T = 36°C, τ_m = 50 ms). The d_{NN} assignment pathway for the α-helical segment 53 to 59 is represented by vertical and horizontal lines connecting consecutive sequential cross peaks (encircled). The arrows below the diagonal indicate the start and the end of the pathway. The amide proton chemical shift positions of residues 53 to 59 are indicated on the left.

3. Results

3.1. *Protein characterization*

Purified rTAP was homogeneous by electrophoresis on 17.25% cross-linking acrylamide gels. Analytical reverse-phase chromatography (Lichrosphere 100, 5 micron, endcapped, 125 × 4 mm, Merck, Darmstadt) showed rTAP eluting as a single peak at 25.4 min using a gradient from 20 to 43% of buffer B in 50 min with a flow rate of 1.6 ml/min. The mass was determined on a PE Sciex API III triple quadrupole mass spectrometer using electrospray ionization, and yielded a value of 6,978.1 (mean of three independent measurements), which is in excellent agreement with the value of 6,978.0 determined from the amino acid composition. Coincidence of the amino acid sequence with that of natural TAP was confirmed by N-terminal amino acid analysis performed on an Applied Biosystems 470A protein sequencer and PTH-amino acid identification from HPLC elution against derivatized amino acid standards [34]. The activity of purified rTAP was determined by its capacity to prolong clotting times on an ACL 300R coagulometer using human plasma, and it was shown to double the APTT (activated partial thromboplastin time) and the PT (thromboplastin time) at 1.9 μM and 4.2 μM, respectively. In addition, it was shown to inhibit the activity of bovine factor Xa (Sigma, St. Louis) with a K_i value of 16 nM, using the factor Xa substrate Chromozym X (Boehringer Mannheim) [35].

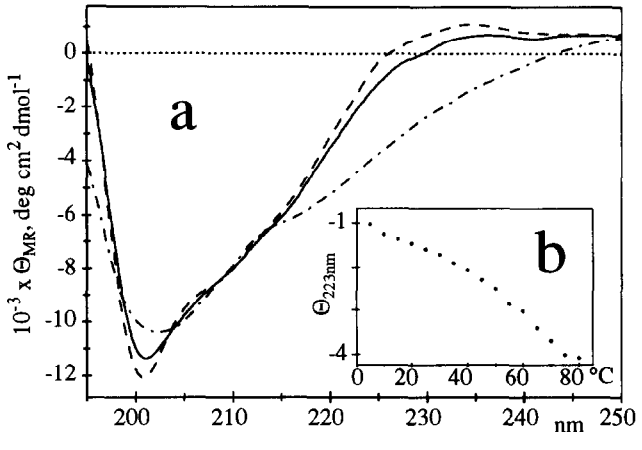

Fig. 1. (a) CD spectra of rTAP at different temperatures: dashed line 10°C, solid line 36°C, dotted-dashed line 80°C. (b) Plot of the ellipticity at 223 nm vs. temperature.

Circular dichroism (CD) spectra of rTAP were recorded on a JASCO J-710 spectropolarimeter in 20 mM sodium phosphate at pH 3.6. Increase of the negative ellipticity near 220 nm

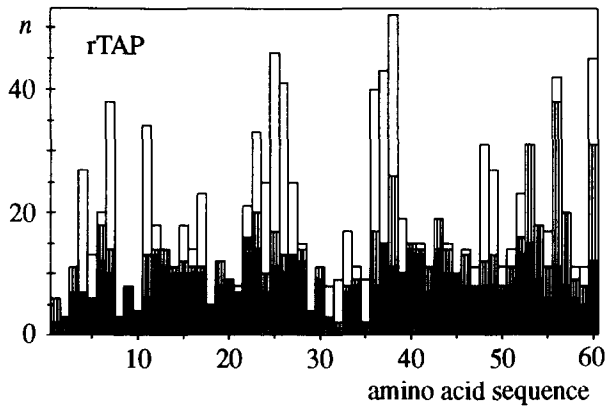

Fig. 3. Plot vs. the amino acid sequence of the number, n, and types of NOE constraints per residue used in the calculation of the solution structure of rTAP. The following code is used to define the different ranges of the NOE constraints: black, intraresidual; cross-hatched, sequential; vertically hatched, medium-range; white, long-range.

upon heating of the sample indicates secondary structure changes (Fig. 1a) with a broad reversible transition centered around 55°C (Fig. 1b). Based on the denaturation curve in Fig. 1b we attempted to work at the lowest possible temperature. However, at temperatures of 25°C or below, rTAP in aqueous solution at pH 3.6 gave very broad ^{1}H NMR lines, probably because of self-aggregation. In the pH range 4.0–5.5 the protein precipitated, and at pH 6.5 we obtained only poor quality ^{1}H NMR spectra. Therefore we eventually decided to proceed with the structure determination at pH 3.6 and 36 °C. Fig. 2 illustrates that ^{1}H NMR spectra of good quality were obtained under these conditions, which are representative of a folded, globular protein.

3.2. ^{1}H NMR assignments

Sequence-specific ^{1}H NMR assignments for rTAP were obtained using standard methods for small proteins [36], with computer support utilizing the program XEASY. As an illustration, Fig. 2 shows the sequential assignments for residues 53–59 in the C-terminal α-helix. The complete chemical shift list for the backbone amide protons and all non-labile hydrogen atoms is presented in the Appendix, which also includes assignments for numerous labile side chain protons.

3.3. Survey of conformational constraints and structure calculation

803 NOE cross peaks were unambiguously assigned and integrated. 658 NOE distance constraints resulted after elimination of the irrelevant constraints (Fig. 3). Coupling constants $^3J_{HN\alpha}$ were obtained for 47 residues, and values of $^3J_{\alpha\beta}$ were obtained for 42 residues. The intraresidual and sequential NOE distance constraints combined with the $^3J_{HN\alpha}$ and $^3J_{\alpha\beta}$ coupling constants yielded a total of 142 dihedral angle constraints (52 for ϕ, 52 for φ and 38 for χ^1) when analyzed with the program HABAS. Individual assignments were obtained for 13 pairs of diastereotopic substituents (see the Appendix), using the programs HABAS and GLOMSA. An overview of the results of the structure calculation after energy minimization of the DIANA conformers is provided in Table 1.

3.4. The three-dimensional structure of rTAP

The polypeptide backbone fold of rTAP is shown in Fig. 4. The elements of regular secondary structure in rTAP consist of a twisted two-stranded antiparallel β-sheet with residues 22–28 and 32–38, and an α-helix comprising residues 51–60. The polypeptide segments 1–3, 8–10, 18–20 and 29–30 are less well defined than the rest of the polypeptide backbone, and they also have low density of NOE distance constraints (Fig. 3). The average of the pairwise global RMSD values relative to the mean structure calculated for the backbone atoms N, C^α and C′ of residues 4–7, 11–17, 21–28 and 31–60 is 0.96 Å (Table 2); when including also the side chains of the 23 residues with the 'best-defined' side chains (those for which the side chain displacements after global backbone superposition are smaller than 2.0 Å, see Table 2 and Fig. 5) the RMSD value increases only slightly to 1.00 Å. The side chains of Trp^{11}, Phe^{26}, Phe^{36}, Ile^{38}, Tyr^{48} and Tyr^{49} exhibit an outstandingly large number of long-range NOEs (Fig. 3), and a close inspection of the three-dimensional structure reveals that these residues are the principal components of the hydrophobic core of rTAP.

The exchange of backbone amide protons with the solvent is rather fast. After 5 h in ^2H_2O at 36°C and p^{2}H 3.6, all labile protons in the protein were completely replaced by deuterions. Fig. 6 shows that the residues with slowed amide proton exchange are all located in polypeptide segments for which the spatial structure is well defined by the NMR data (Table 2). They are mostly amide protons that form the characteristic hydrogen bonds in the regular secondary structure elements, namely Ala^{24}, Phe^{26}, Asp^{34}, Phe^{36} and Ile^{38} in the β-sheet, and Cys^{55}, Phe^{56}, Asn^{57}, Ala^{58} Cys^{59} and Ile^{60} in the α-helix. These regular hydrogen bonds are highly populated among the 20 conformers that represent the NMR structure (Table 3). Residue Tyr^{25}, which has a slowly exchanging amide proton, is related by NOEs with the slowly exchanging amide proton of Tyr^{49}, showing that Tyr^{25} forms a one-residue, third antiparallel β-strand, which is a feature that was previously also reported for BPTI [26,37].

rTAP contains 11 side chain carboxylates in addition to the C-terminus, whereas positive charges are located on the N-terminus, 7 Arg and Lys, and one His. It is thus an acidic protein with an isoelectric point of about 4.5. The β-sheet in-

Table 1
Analysis of the 20 DIANA conformers of rTAP with the lowest residual target function values

Quantity	Average value ± S.D.[a]
Target function (Å^2)	8.6 ± 3.1
AMBER energy (kcal/mol)	− 1646 ± 84
NOE constraint violations:	
sum (Å)	14.3 ± 1.0
maximum (Å)	0.2 ± 0.0
Dihedral angle constraint violations:	
number > 5°	1.2 ± 1.6
sum (deg)	53.0 ± 12.6
maximum (deg)	5.4 ± 0.8

[a]Average values and standard deviations are listed for the group of 20 conformers. In the structure calculations the weighting factors for the NOE upper distance constraints were 1, for the van der Waals lower distance limits 2, and for dihedral angle constraints 5 Å^2. The target function value is given for the 20 DIANA conformers before energy minimization, all other data are for the same group of conformers after energy-refinement with the program OPAL.

cludes 2 positively and 2 negatively charged side chains, the α-helix one of each, but the large majority of the charged groups are observed in the loop regions outside of the regular secondary structures (Fig. 6). In the global three-dimensional structure there is a pronounced asymmetric charge distribution. In the standard orientation (Figs. 4 and 5) the negatively charged groups are crowded in the upper half of the molecule (residues 10–19 and 41–47), and there is a clear-cut surplus of positive charges in the lower half (residues 1–9, 30, 53) (Fig. 7).

The residues Asp[10], Thr[44], Ser[50], Ala[58], Cys[59] and Ile[60] exhibit strong d_{NN} sequential NOE connectivities and have at the same time large values of the $^3J_{HN\alpha}$ coupling constant. In particular for the C-terminal tripeptide segment 58–60, for which the patterns of sequential and medium-range NOE connectivities suggest that these residues belong to the α-helix, the observation of $^3J_{HN\alpha}$ values larger than 7.0 Hz was unexpected. These apparent inconsistencies [36] may manifest increased local mobility of the protein under the experimental conditions used (see Fig. 1).

The atomic coordinates of the 20 energy-minimized DIANA conformers used to represent the solution structure of rTAP have been deposited in the Brookhaven data bank, together with the complete input of conformational constraints used for the structure calculation.

4. Discussion

The rTAP sequence includes features that are reminiscent of some sequence properties of the large family of Kunitz-type protein proteinase inhibitors. These proteins, and particularly BPTI, have been the subject of detailed conformational studies by X-ray crystallography [37–39] as well as NMR [26,40,41]. A sequence alignment of the five members of this protein family for which a three-dimensional structure is available, i.e. BPTI [26], Toxin K [41], α-DTX [39], APPI [38] and ShPI [40], shows identical spacing of the cysteinyl residues, and a detailed structure comparison revealed only minor conformational differences [40], indicating that the protease inhibitory activities of BPTI, APPI and ShPI rely probably on identical inhibitory mechanisms. In this section we attempt to gain further insight into possible structure-function correlations in rTAP by comparison with BPTI.

Although the disulfide bond pattern of rTAP, 5–59, 15–39 and 33–55 [31], resembles that of the Kunitz-type inhibitors, no

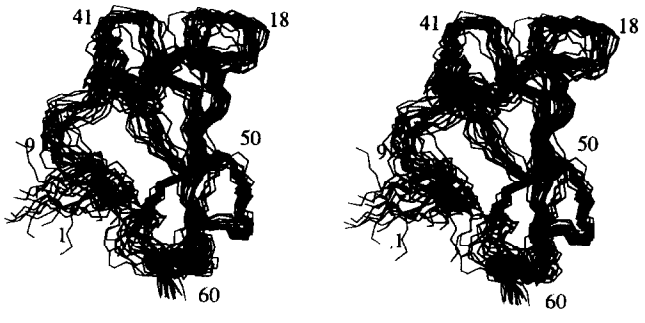

Fig. 4. Stereo view of the polypeptide backbone of the 20 final, energy-refined DIANA conformers used to represent the NMR structure of rTAP in solution. The backbone atoms N, C^α and C′ of the residues 4–7, 11–17, 21–28 and 31–60 of the conformers 1 to 20 were superimposed for minimal RMSD with the mean structure (Table 2). Some C^α positions are identified with the sequence numbers.

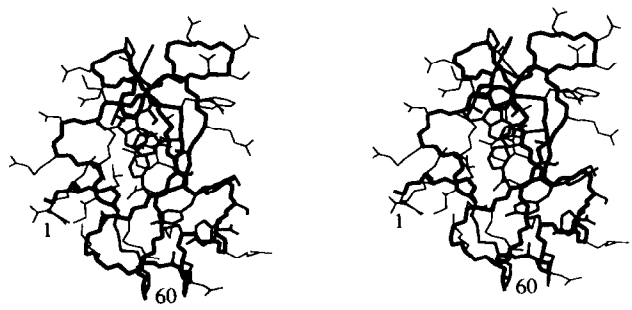

Fig. 5. Stereo view of an all-heavy-atom representation of one of the energy-refined conformers of rTAP in the same orientation as in Fig. 4. The polypeptide backbone atoms N, C^α and C′ are connected with a thick line. Best-defined side chains as listed in Table 2 are drawn with medium lines, the other side chains with thin lines. The locations of the chain-terminal residues 1 and 60 are also indicated.

significant level of sequence homology could be detected (Fig. 6). The three-dimensional structures of BPTI and rTAP show good superposition of the regular secondary structure elements and the dipeptide segment preceding the α-helix (Fig. 8), which contains the corresponding residues Phe[45] in BPTI and Tyr[49] in rTAP. The side chains of these two residues are similarly oriented relative to other molecular regions in the two proteins, and show similar patterns of long-range NOEs to both the α-helix and the β-sheet. Outside of these regions the fold of rTAP differs considerably from that of the common Kunitz-type protease inhibitors. The close fit of the regular secondary structure elements (Fig. 8) along with insertions and deletions of polypeptide segments immediately before and after the β-sheet enforces large structural differences. In BPTI, the second strand of the β-sheet extends up to residue 35, and it is followed by the tripeptide segment Gly-Gly-Cys in an extended conformation, with Cys[38] forming a disulfide bridge with Cys[14], which is the residue preceding the active site. A sequence alignment of all the proteins which are classified as BPTI/Kunitz-

Table 2
RMSD values calculated for different atom selections in the solution structure of rTAP

Atoms used for comparison[a]	RMSD (Å) ± S.D.[b]
bb (1–60)	1.37 ± 0.22
bb (4–7, 11–17, 21–28, 31–60)	0.96 ± 0.17
Same + best-defined side chains[c]	1.00 ± 0.17
All heavy atoms (4–7, 11–17, 21–28, 31–60)	1.48 ± 0.20
bb (20–28, 32–38, 51–60)[d]	0.60 ± 0.10
bb rTAP mean (22–28, 32–38, 51–60) with bb BPTI mean (18–24, 29–35, 47–56)[d]	0.99

[a]bb stands for the backbone heavy atoms N, C^α and C′. The numbers in parentheses indicate the residues for which the RMSD was calculated.
[b]Averages are given of the pairwise RMSD values between each of the 20 energy-refined DIANA conformers and the mean solution structure. RSMD values were calculated with the program XAM [44].
[c]Best-defined side chains are those with global displacements smaller than 2.0 Å and include the following 23 residues: 5, 11, 15, 24–26, 35, 36, 38–40, 43, 44, 49–52, 54–56, 58–60.
[d]These residues form the antiparallel β-sheet and the α-helix. For the comparison of rTAP with BPTI the mean coordinates of the NMR structures of the two proteins were used, and the superposition is for the best fit of the β-sheet and the α-helix.

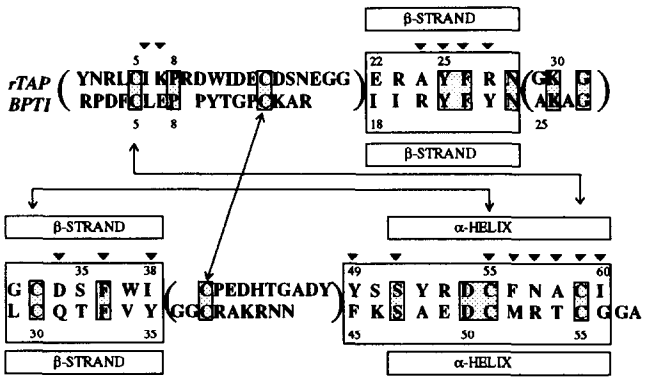

Fig. 6. Tentative partial alignment of the amino acid sequences of rTAP and BPTI based on the assumption that the cysteinyl residues are in corresponding positions. Sequence identities are indicated by shaded boxes. Larger boxes indicate regions with near-identity of the three-dimensional structure (see Fig. 8). Outside of these large boxes, parentheses indicate segments for which no satisfactory alignment could be obtained either using sequence arguments or three-dimensional structure arguments. Arrows indicate the disulfide bond pairings. The regular secondary structure elements are indicated above and below the respective sequences.Triangles above the rTAP sequence indicate residues with observably slow amide proton exchange at 36°C and pH 3.6 (see text).

type proteinase inhibitor homologs in the SwissProt sequence database shows that the residue preceding Cys in the above tripeptide segment is a strictly conserved glycine. Furthermore, the local backbone conformation of this residue in the three-dimensional structure of BPTI can only be satisfied by a glycine. In rTAP the second β-sheet extends up to residue 38, and the residues corresponding to Gly[36] and Gly[37] in BPTI are missing. As a result, Cys[39], which forms a disulfide bond with Cys[15], is situated immediately after the second strand of the β-sheet (Fig. 6). This enforces different locations of this disulfide bond in the two molecules, and the conformations of the two loops that are connected by this disulfide bond are widely different in the two proteins (Fig. 8).

Overall the picture emerging is that of an amazingly faithful conservation of a structural scaffold between rTAP and the Kunitz-type inhibitors, which consists of the β-sheet and the α-helix (Fig. 8). This scaffold supports distinctly different connecting loop regions, which are presumably responsible for conferring different functional properties to the two types of molecules.

In earlier work [14] it was found that a mutation of Asp[16] in rTAP to Arg or Lys, which corresponds to conservation of the residue type in the corresponding position of BPTI, does not result in a rTAP mutant with inhibitory activity against trypsin. In view of the different loop structures carrying this residue position in the two proteins (Fig. 8), and also considering the crowding with negative charges of the rTAP region corresponding to the active site in BPTI (Fig. 7), this result can readily be rationalized on the basis of the three-dimensional structure. Similarly, previous site-directed mutagenesis studies indicated two regions of rTAP that contribute to the high-affinity binding interaction with factor Xa. The first comprises the three N-terminal residues and constitutes the primary binding determinant [14]. This N-terminal tripeptide shows only few NOE distance constraints (Fig. 3), appears to be flexibly disordered and probably adopts a defined conformation only upon binding to the enzyme. A region between residues 40 and 54 constitutes a probable secondary binding determinant [14]. The presently described three-dimensional structure shows clearly that neither of these two binding regions are located near the position corresponding to the protease-binding site in BPTI, implicating distinctly different inhibitory mechanisms for rTAP and BPTI.

Despite the similarity of the secondary structure elements of rTAP and BPTI, the amide proton exchange in rTAP is many orders of magnitude faster than in BPTI [42]. Past experience with a variety of Kunitz-type inhibitors [43] implies that the

Table 3
Backbone–backbone hydrogen bonds identified in the solution structure of rTAP

Donor[a]	Acceptor[a]	Conformers[b]
14 Glu NH	12 Ile O′	13
19 Glu NH	17 Ser O′	11
24 Ala NH	36 Phe O′	18
25 Tyr NH	49 Tyr O′	12
26 Phe NH	34 Asp O′	12
27 Arg NH	5 Cys O′	19
28 Asn NH	32 Gly O′	11
30 Lys NH	28 Asn O′	10
34 Asp NH	26 Phe O′	18
38 Ile NH	22 Glu O′	14
55 Cys NH	51 Ser O′	14
56 Phe NH	52 Tyr O′	20
57 Asn NH	53 Arg O′	20
58 Ala NH	54 Asp O′	19
59 Cys NH	55 Cys O′	18
60 Ile NH	56 Phe O′	20

[a]NH and O′ stand for the backbone amide protons and carbonyl oxygens. Residues with slowly exchanging amide protons at p²H 3.6 and 36°C are indicated in bold face.
[b]In each individual conformer a hydrogen bond is identified if the proton–acceptor distance is less than 2.4 Å, and the angle between the donor–proton bond and the line connecting the donor and acceptor atoms is less than 35°. Hydrogen bonds are reported if this criterion is met in at least 10 of the 20 energy-refined DIANA conformers of rTAP. This column lists the number of conformers that fulfil the above criteria.

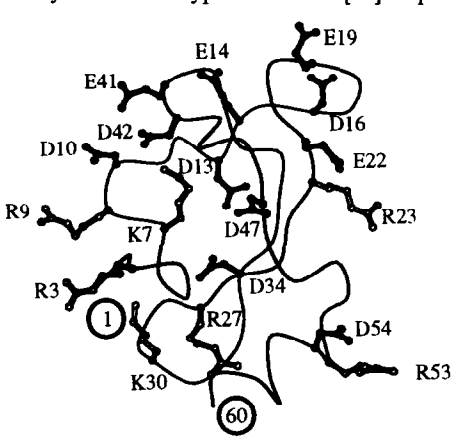

Fig. 7. Ribbon drawing of rTAP showing the locations of charged groups. Same orientation as in Fig. 4. The backbone is represented by a thin line. Arg or Lys side chains, and Asp or Glu side chains, respectively, are represented by open and filled ball and stick drawings, and the individual residues are identified with the one-letter amino acid symbols and the sequence locations. The two chain ends are indicated with encircled numbers.

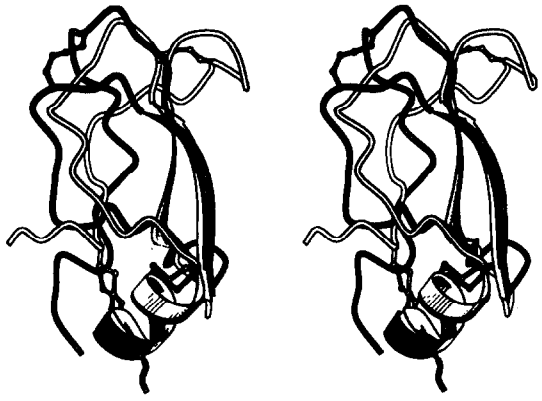

Fig. 8. Superposition of ribbon drawings of the rTAP and BPTI mean NMR structures generated with the program MOLSCRIPT [45] after fit for minimal RMSD of the residues corresponding to positions 22–28, 32–38 and 51–60 in rTAP (Table 2). Dark gray shading corresponds to BPTI, and rTAP is white. The disulfide bonds are represented by ball and stick drawings.

extent of this difference cannot simply be related to the difference in thermal stability of the two proteins. Furthermore, in contrast to BPTI, all the aromatic ring undergo rapid flipping motions about the C^{β}–C^{γ} bond (Table A1), which indicates increased internal mobility [36]. It remains to be seen whether these features are yet another structural determinant of the implicated different modes of action of the two classes of inhibitors.

With regard to the so far rather elusive inhibitory mechanism of rTAP, further studies are planed in collaboration with the group of Prof. R. Huber, MPI Martinsried, to investigate possible contact sites by molecular modeling using the present rTAP structure and the crystal structure of factor Xa [15].

Acknowledgments: We wish to thank Dr. F. Buxton and R. Grossenbacher for yeast strain development and expression, R. Voellmy for large scale purifications, R. Knecht for N-terminal sequencing, Dr. D. Müller for mass spectral analysis and Dr. T. Szyperski for help with the acquisition of the NMR spectra. Financial support by the Schweizerischer Nationalfonds (Project 31. 32033. 91) and by a Bundesstipendium to W.A., and the use of the Cray Y-MP computer of the ETH Zürich are gratefully acknowledged.

References

[1] Andersson L. and Lundé R. (1979) in: Plasma Proteins (Blombäck, B. and Hanson, L.Å., Eds.) pp. 221–304, Wiley, New York.
[2] Furie, B. and Furie, B.C. (1988) Cell 53, 505–518.
[3] Markwardt, F. (1970) Methods Enzymol. 19, 924–932.
[4] Folkers, P.J.M., Clore, G.M., Driscoll, P.C., Dodt, J., Köhler, S. and Gronenborn, A.M. (1989) Biochemistry 28, 2601–2617.
[5] Haruyama, H. and Wüthrich, K. (1989) Biochemistry 28, 4301–4312.
[6] Szyperski, T., Güntert, P., Stone, S.R. and Wüthrich, K. (1992) J. Mol. Biol. 228, 1193–1205.
[7] Grütter, M.G., Priestle, J.P., Rahuel, J., Grossenbacher, H., Bode, W., Hofsteenge, J. and Stone, S.R. (1990) EMBO J. 9, 2361–2365.
[8] Rydel, T.J., Tulinsky, A., Bode, W. and Huber, R. (1991) J. Mol. Biol. 221, 583–601.
[9] Nutt, E., Gasic, T., Rodkey, J., Gasic, G.J., Jacobs, J.W., Friedman, P.A. and Simpson, E. (1988) J. Biol. Chem. 263, 10162–10167.
[10] Blankenship, D.T., Brankamp, R.G., Manley, G.D. and Cardin, A.D. (1990) Biochem. Biophys. Res. Commun. 166, 1384–1389.
[11] Kido, H., Yokogoshi, Y. and Katunuma, N. (1988) J. Biol. Chem. 263, 18104–18107.
[12] Waxman, L., Smith, D.E., Arcuri, K.E. and Vlasuk, G.P. (1990) Science 248, 593–596.
[13] Jordan, S.P., Mao, S., Lewis, S.D. and Shafer, J.A. (1992) Biochemistry 31, 5374–5380.
[14] Dunwiddie, C.T., Neeper, M.P., Nutt, E.M., Waxman, L., Smith, D.E., Hofmann, K.J., Lumma, P.K., Garsky, V.M. and Vlasuk, G.P. (1992) Biochemistry 31, 12126–12131.
[15] Padmanabhan, K., Padmanabhan, K.P., Tulinsky, A., Bode, W., Huber, R., Blankenship, D.T., Cardin, A.D. and Kisiel, W. (1993) J. Mol. Biol. 232, 947–966.
[16] Butt, T.R., Sternberg, E.J., Gorman, J.A., Clark, P., Hamer, D., Rosenberg, M. and Crooke, T.S. (1984) Proc. Natl. Acad. Sci. USA 81, 3332–3336.
[17] Rance, M., Sørensen, O., Bodenhausen, G., Wagner, G., Ernst, R.R. and Wüthrich, K. (1983) Biochem. Biophys. Res. Commun. 117, 479–485.
[18] Griesinger, C., Otting, G., Wüthrich, K. and Ernst, R.R. (1988) J. Am. Chem. Soc. 110, 7870–7872.
[19] Anil-Kumar, Ernst, R.R. and Wüthrich, K. (1980) Biochem. Biophys. Res. Commun. 95, 1 6.
[20] Müller, N., Ernst, R.R. and Wüthrich, K. (1986) J. Am. Chem. Soc. 108, 6482–6492.
[21] Wagner, G. and Zuiderweg, E.R.P. (1983) Biochem. Biophys. Res. Commun. 113, 854–860.
[22] Otting, G., Orbons, L.P.M. and Wüthrich, K. (1990) J. Magn. Reson. 89, 423–430.
[23] Szyperski, T., Güntert, G., Otting, G. and Wüthrich, K. (1992) J. Magn. Reson. 99, 552–560.
[24] Griesinger, C., Sørensen, O.W. and Ernst, R.R. (1985) J. Am. Chem. Soc. 107, 6394–6396.
[25] Güntert, P. and Wüthrich, K. (1992) J. Magn. Reson. 96, 403–407.
[26] Berndt, K.D., Güntert, P., Orbons, L.P.M. and Wüthrich, K. (1992) J. Mol. Biol. 227, 757–775.
[27] Güntert, P., Braun, W. and Wüthrich, K. (1991) J. Mol. Biol. 217, 517–530.
[28] Güntert, P., Braun, W., Billeter, M. and Wüthrich, K. (1989) J. Am. Chem. Soc. 111, 3997–4004.
[29] Güntert, P. and Wüthrich, K. (1991) J. Biomol. NMR 1, 447–456.
[30] Güntert, P., Berndt, K.D. and Wüthrich, K. (1993) J. Biomol. NMR 3, 601–606.
[31] Sardana, M., Sardana, V., Rodkey, J., Wood, T., Assunta, N., Vlasuk, G.P. and Waxman, L. (1991) J. Biol. Chem. 266, 13560–13563.
[32] Williamson, M.P., Havel, T.F. and Wüthrich, K. (1985) J. Mol. Biol. 182, 295–315.
[33] Weiner, P.K., Kollman, P.A., Nguyen, D.T. and Case, D.A. (1986) J. Comp. Chem. 7, 230–252.
[34] Hunkapiller, M.W., Grundlund-Moyer, K. and Whiteley, N.W. (1986) in: Methods of Protein Microcharacterization (Shively, J.E. Ed.) pp. 315–327, Humana Press, Clifton, NJ.
[35] Kolde, H.J. and Bruhn, H.D. (1983) Laboratoriumsblätter 33, 99–106.
[36] Wüthrich, K. (1986) NMR of Proteins and Nucleic Acids, Wiley, New York.
[37] Deisenhofer, J. and Steigemann, W. (1975) Acta Crystallogr. B31, 238–250.
[38] Ponte, P., González-DeWhitt, P., Schilling, J., Miller, J., Hsu, D., Greenberg, B., Davis, K., Wallace, W., Lieberberg, I., Fuller, F. and Cordell, B. (1988) Nature 331, 525–527.
[39] Skarzynski, T. (1992) J. Mol. Biol. 224, 671–683.
[40] Antuch, W., Berndt, K.D., Chávez, M.A., Delfín, J. and Wüthrich, K. (1993) Eur. J. Biochem. 212, 675–684.
[41] Berndt, K.D., Güntert, P. and Wüthrich, K. (1993) J. Mol. Biol. 234, 735–750.
[42] Wagner. G. and Wüthrich, K. (1982) J. Mol. Biol. 160, 343–361.
[43] Wagner, G. and Wüthrich, K. (1978) Nature 275, 247–248.
[44] Xia, T.H. (1992) Software for Determination and Visual Display of NMR Structures of Proteins: the Distance Geometry Program DGPLAY and the Computer Graphics Programs CONFOR and XAM, Ph.D. Thesis, ETH Zürich, Switzerland.
[45] Kraulis, P.J. (1991) J. Appl. Crystallogr. 24, 946 950.

Appendix

Table A1
^{1}H NMR chemical shifts of rTAP in aqueous solution at pH 3.6 and T = 36°C

Residue		Chemical shift (ppm)*			
		NH	αH	βH	Others
Tyr	1		4.24	3.11, 3.11	δH 7.05, 7.05; εH 6.75, 6.75
Asn	2	8.42	4.67	2.77, 2.92	δNH_2 6.93, 7.54
Arg	3	8.40	4.09	1.40, 1.49	γCH_2 1.41; δCH_2 2.80, 2.88; εNH 6.99
Leu	4	8.20	4.33	1.42, 1.75	γH 1.64; δCH_3 0.66, 0.71
Cys	5	8.18	4.85	2.87, 3.08	
Ile	6	7.43	4.33	1.72	γCH_2 1.40, 1.10; γCH_3 0.71; δCH_3 0.75
Lys	7	8.23	2.22	0.34, 0.96	γCH_2 −0.12, 0.60; δCH_2 0.52, 0.60; εCH_2 2.10, 2.21
Pro	8		4.04	1.24, 2.08	γCH_2 1.58; δCH_2 2.04, 3.22
Arg	9	8.32	3.85	1.70, 1.70	γCH_2 1.58; δCH_2 3.11; εNH 7.08
Asp	10	8.13	4.55	2.73, 2.85	
Trp	11	7.32	4.47	2.87, 2.94	δ^1H 6.86; ε^3H 7.08; ε^1NH 9.92; ζ^2H 7.31; ζ^3H 6.80; η^2H 6.75
Ile	12	7.90	4.27	1.65	γCH_2 1.29, 1.11; γCH_3 0.81; δCH_3 0.75
Asp	13	8.55	4.89	2.83, 2.88	
Glu	14	7.79	4.64	2.00, 1.86	γCH_2 2.13, 2.31
Cys	15	7.94	4.75	3.04, 2.99	
Asp	16	8.13	4.19	2.60, 2.65	
Ser	17	7.90	3.90	3.59, 3.45	
Asn	18	8.03	4.52	2.70	δNH_2 6.77, 7.42
Glu	19	7.77	4.29	2.12, 1.83	γCH_2 2.32
Gly	20	7.88	3.81, 3.99		
Gly	21	7.94	3.89, 4.17		
Glu	22	8.23	4.57	1.88, 2.06	γCH_2 2.36
Arg	23	8.19	4.28	0.87, 1.15	γCH_2 0.69, 0.78; δCH_2 2.62, 2.70; εNH 6.76; ηNH_2 6.40
Ala	24	8.60	4.86	0.88	
Tyr	25	7.88	5.11	2.25, 2.40	δH 6.54, 6.54; εH 6.66, 6.66
Phe	26	8.39	4.99	2.45, 3.29	δH 6.82, 6.82; εH 6.63, 6.63; ζH 6.27
Arg	27	9.05	4.64	1.76, 1.76	γCH_2 1.56; δCH_2 2.96; εNH 7.14
Asn	28	8.38	4.97	3.21, 2.62	δNH_2 7.14, 7.66
Gly	29	8.53	3.94, 4.01		
Lys	30	8.43	4.58	1.48, 1.95	γCH_2 1.24; δCH_2 1.60; εCH_2 2.92
Gly	31	8.28	3.67, 4.26		
Gly	32	7.91	3.94, 4.56		
Cys	33	7.30	5.60	3.21, 2.74	
Asp	34	9.15	5.13	2.64, 2.68	
Ser	35	8.14	4.51	2.88, 2.88	
Phe	36	8.78	4.52	2.69, 3.16	δH 7.20, 7.20; εH 7.26, 7.26; ζH 7.17
Trp	37	8.30	4.70	2.87, 3.28	δ^1H 7.19; ε^3H 7.32; ε^1NH 9.89; ζ^2H 7.36; ζ^3H 6.90; η^2H 7.13
Ile	38	8.56	4.29	1.67	γCH_2 0.95, 1.55; γCH_3 0.68; δCH_3 0.55
Cys	39	8.32	4.91	2.54, 3.25	
Pro	40		4.08	1.87, 2.25	γCH_2 1.97, 2.08; δCH_2 3.72, 3.79
Glu	41	8.56	4.06	1.77, 1.99	γCH_2 2.35
Asp	42	7.75	4.49	2.33, 2.13	
His	43	7.77	4.70	3.14, 3.23	δ^2H 7.14; ε^1H 8.40
Thr	44	8.12	4.34	4.31	γCH_3 1.20
Gly	45	8.45	3.77, 4.01		
Ala	46	7.70	4.23	1.12	
Asp	47	8.06	4.60	2.61, 2.49	
Tyr	48	7.26	4.36	3.13, 2.58	δH 7.11, 7.11; εH 6.83, 6.83
Tyr	49	9.97	4.55	2.75, 3.06	δH 7.08, 7.08; εH 6.50, 6.50
Ser	50	9.16	4.92	4.25, 3.93	
Ser	51	7.37	4.33	3.87, 3.76	
Tyr	52	8.15	2.85	2.55, 2.64	δH 6.82, 6.82; εH 6.77, 6.77
Arg	53	8.35	3.73	1.60, 1.82	γCH_2 1.52; δCH_2 3.11; εNH 7.08
Asp	54	7.31	4.23	2.50, 2.67	
Cys	55	6.89	3.16	2.74, 2.67	
Phe	56	8.97	3.50	2.38, 2.76	δH 6.95, 6.95; εH 7.38, 7.38; ζH 7.29
Asn	57	8.06	4.29	2.69, 2.74	δNH_2 6.67, 7.58
Ala	58	7.10	4.32	1.22	
Cys	59	8.19	4.82	2.87, 2.87	
Ile	60	7.11	3.90	1.47	γCH_2 0.82, 1.00; γCH_3 0.58; δCH_3 0.43

*The chemical shifts are in ppm relative to internal sodium [2,2,3,3-$^2H_4$]-3-trimethylsilylpropionate. For methylene groups two chemical shifts are given only when two separate resonance lines were observed or the presence of two degenerate resonances was evidenced by 2Q spectroscopy. Individual assignments for pairs of diastereotopic substituents obtained using the programs HABAS and GLOMSA are indicated by underlined chemical shift values. The chemical shift of the proton with the lower branch number is listed first, e.g. the β^2 proton.